DESIGN OF THE LOW ENERGY BEAM TRANSPORT LINE FOR THE JAEA-ADS LINAC

B. Yee-Rendon*, Y. Kondo, J. Tamura, F. Maekawa and S. Meigo
Japan Atomic Energy Agency (JAEA), Tokai, Japan

Abstract

The Japan Atomic Energy Agency (JAEA) is proposing a 30-MW proton linear accelerator (linac) for the application of accelerator-driven subcritical system (ADS) technology to achieve nuclear waste transmutation. A major challenge for the JAEA-ADS linac is the efficient transport of a 35 keV proton beam from the ion source to the radio-frequency quadrupole. In order to achieve this goal, we have optimized a magnetostatic low energy beam transport (LEBT) consisting of two solenoids to reduce the transmission of high-charge ions generated by the source and minimize the growth of proton emittance, while taking into account different values of space-charge compensation along the LEBT. In this report, we present the optical design and discuss the multiparticle tracking results of the JAEA-ADS LEBT.

INTRODUCTION

The Japan Atomic Energy Agency (JAEA) is designing an accelerator-driven subcritical system (ADS) for transmuting minor actinides [1]. The JAEA-ADS proposal uses a 30-MW proton beam to produce spallation neutrons for an 800-MWth thermal power subcritical reactor. JAEA-ADS accelerator team has completed most of the linac design [2–5]. This work focuses on the design of the low energy beam transport (LEBT) that carries a 25 mA proton beam from the ion source to the RFQ.

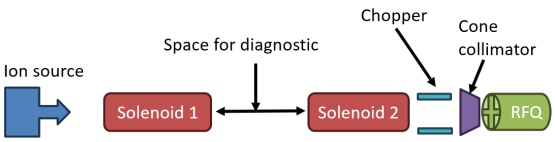

Figure 1: Schematic view of the JAEA-ADS LEBT design.

The schematic design of the JAEA-ADS LEBT is depicted in Fig. 1, the design is composed by two solenoids, chopper, conical collimator, and beam diagnostics. Table 1 offers a summary of the major parameters and their corresponding requirements for the JAEA-ADS LEBT. The design of LEBT was formulated for steady-state operation, i.e., without a chopper, in order to use constant space-charge compensation. Additionally, the the model employed 3D-EM solenoid fields to consider the effect of non-linear magnetic fields. The current solenoid scans were applied to establish appropriate configurations that were subsequently employed as input for the RFQ models to verify their compatibility. The manuscript outlines the criteria, simulations, and results for the JAEA-ADS LEBT.

* byee@post.j-parc.jp

Table 1: Main Parameters for the JAEA-ADS LEBT. The Requirements for the Two Developed RFQ Models: Reference [3] and Equipartioned (EP) [4] are Presented.

Parameter		
Particle	Proton	
Beam current (mA)	25	
Beam energy (keV)	35	
$\varepsilon_{rms,norm,trans}$ (π mm mrad)	≤ 0.2	
Length (m)	≤ 2	
RFQ models	Reference	EP
α	1.29	2.9
β (mm/πmrad)	0.06	0.12

OPTICS DESIGN

At low energy, high-intensity beams experience significant self-generated repulsion between charged particles, known as space-charge. This leads to irreversible emittance growth, resulting in increased beam size and ultimately loss of the beam. However, in regions where the beam propagates in the presence of residual gas, the gas molecules become ionized by the beam. The ionized secondary particles that carry an opposite charge to the beam are trapped and accumulated in the beam potential until reaching an equilibrium. The net effect is a reduction of the self-repulsion of the beam particles, the so-called space-charge compensation [6].

In this work, we focus on designing the LEBT for steady-state operation, where space-charge compensation reaches equilibrium. The compensation depends on residual gas pressure and EM field, e.g., ionized secondary particles are not easily accumulated inside the beam in the presence of electrostatic fields. Therefore, the space-charge compensation usually changes along the LEBT.

In our case, we assumed a constant space-charge compensation by section. This was done to assumed a more reasonable model. To this end, we used the space-charge compensation degree (η) different in each part, where η=100% means that the beam is fully space-charge compensated and 0%, the beam experience the full space-charge effects.

Figure 2 presents the space-charge model used in this study. η starts with a small value and increases towards the first solenoid. Then, η reaches a large value (usually assuming > 85%). Finally, η decreased at the entrance of the RFQ. The values used are more conservative than the employed by other LEBTs [7, 8] in order to achieve a more robust design [9].

LEBT design should also avoid non-linear magnetic fields to reduce beam loss and limit emittance growth. Addition-

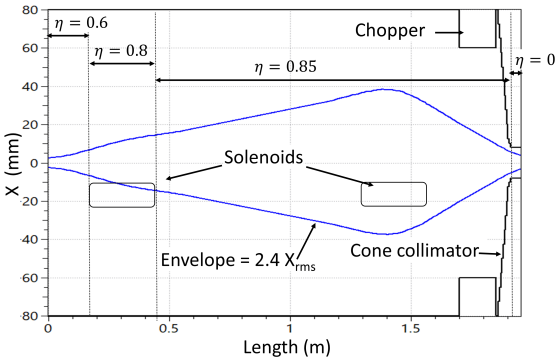

Figure 2: Steady-state JAEA-ADS LEBT envelope design. The model assumed a constant space-charge section by sections.

ally, the solenoids must be tuned to achieve the required Twiss parameters, i.e., produce a properly converged beam. Solenoid 1 must keep and adequate beam size until Solenoid 2. Then, Solenoid 2 should smoothly produce a convergence beam at the end of the LEBT. The chopper was not used in this analysis since the beam steady-state condition was simulated.

SOLENOID MODEL

Design and tuning of the solenoids play a major role in achieving a robust and efficient LEBT. Thus, we developed a model that uses analytic calculation and 3D-EM simulations for the solenoid design. 3D-EM fields allow us to consider non-linear effects that are presented in real solenoids. Additionally, this tool assists in achieving solenoid design with a proper spherical aberration to obtain an acceptable beam emittance growth.

The emittance growth due to spherical aberrations in the solenoid is estimated as [10]:

$$\epsilon_{trans}/\epsilon_{trans,0} = \sqrt{1 + k(\frac{C_\alpha R^4}{f\epsilon_{trans,0}})^2}, \quad (1)$$

where ϵ_{trans} is four-times the unnormalized emittance, k is a coefficient that depends on the beam distribution ($k = 0.11$ for uniform beam distribution), C_α is the spherical aberration, R is the maximum transverse size inside the solenoid, and f is the focusing length of the solenoid.

Assuming that the solenoid field is described by:

$$B_z(z) = \frac{B_{peak}}{1 + (z/a)^6}, \quad (2)$$

where B_{peak} is the peak of field and a is the half of the half width to full width; thus, C_α and f can be approximated to:

$$C_\alpha = \frac{1}{2}\frac{\int B_z'^2(z)dz}{\int B_z^2(z)dz} \approx \frac{7}{12a^2}, \quad (3)$$

and

$$f = \frac{(2B\rho)^2}{\int B_z^2(z)dz} \approx \frac{9}{5\pi a}\frac{(2B\rho)^2}{B_{peak}^2}, \quad (4)$$

where $B\rho$ is the beam rigidity.

In addition, Durandeau [11] derived an expression for the B_{peak} as a function of the number of turns, current, and geometry of the solenoid:

$$B_{peak} \approx \frac{\mu_0 NI}{a/0.485}, \quad (5)$$

where μ_0 is the vacuum permeability and NI is the product of the number of coils turns and the coil current.

After substituting Eqs. (3), (4), and (5) into Eq. (1) and performing algebraic operations, the following expression is obtained:

$$\frac{\epsilon_{trans}}{\epsilon_{trans,0}} \approx \sqrt{1 + k(\frac{0.06}{a^3}(\frac{\mu_0 NI}{B\rho})^2\frac{R^4}{\epsilon_{trans,0}})^2}, \quad (6)$$

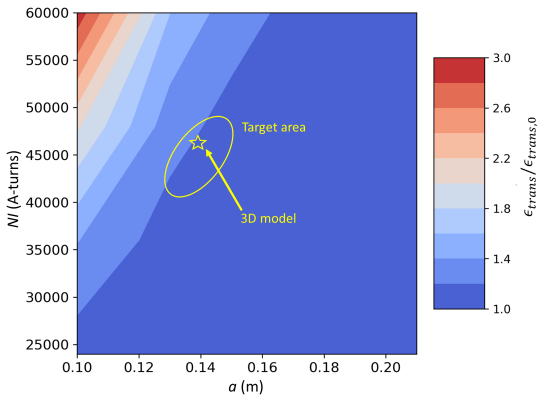

Figure 3: Unnormalized emittance growth map as a function of the parameter a and the products of the number of turns in the coils per current (NI) . The target area (ellipse) and the 3D model (star) are indicated.

Figure 3 shows an unnormalized emittance growth map as a function of the parameter a and NI for the JAEA-ADS LEBT using Eq. (6). For this scan, $\epsilon_{trans,0}$= 46.33 π mm mrad is used according to ion source simulations [5], $B\rho$ is 0.027 Tm for a proton beam with an energy of 35 keV. Additionally, it was assumed a R= 30 mm, and an uniform beam distribution, k = 0.11. A target area was indicated based on preliminary results to achieve a $\frac{\epsilon_{trans}}{\epsilon_{trans,0}} < 1.4$. As a result, the suitable parameters for a are between 120 to 150 mm and for NI, from 4000 to 500 A−turns, which correspond to a B_{peak} between 170 to 220 mT.

Using the CST Studio Suite program [12], a 3D model was created based on the analytic results. The model consists of 6 coils, a shielding yoke made of iron, and a beam pipe with radial and longitudinal mirror symmetry. The coils use hollow cables for water cooling. Figure 4 shows the 3D design, and the optimized Bz field, while the specifications of the model are provided on Table 2. There was an acceptable agreement between analytic and 3D model results.

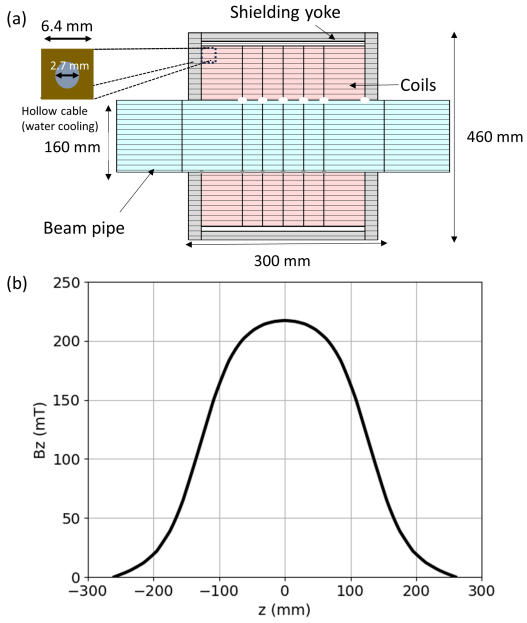

Figure 4: 3D Solenoid model: (a)-subplot presents geometry details of the model and (b)-subplot shows the longitudinal B-field at the center of beam pipe.

Table 2: 3D Solenoid Parameters

Parameter	
Length (mm)	300
External diameter (mm)	460
Aperture diameter (mm)	160
Total number of coil turns	782
Nominal coil current (A)	60
Nominal B_{peak} (mT)	217
a (mm)	130

BEAM DYNAMIC STUDIES

The beam dynamic studies used the output parameters of the extraction system for the JAEA-ADS linac [5] as input parameters. Actual proton sources not only produce proton beams but also other high-charge ions. Therefore, in this work, proton and H_2^+ were simulated. Table 3 presents the input parameters for the LEBT simulations. The beam dynamic studies were done using the TraceWin code [13].

Table 3: Input Parameters for the LEBT Simulations

Parameter	**Proton**	**H_2^+**
Beam energy (keV)	35	
α	-1.73	
β (mm/πmrad)	0.16	
Distribution type	Uniform	
Beam current (mA)	25.06	2.98
$\varepsilon_{rms,norm,trans}$ (π mm mrad)	0.09	0.10
Number of macroparticles	1×10^5	1.2×10^4

Solenoid current scans were implemented to determined the suitable values for the LEBT operations. Figure 5 shows the proton transmission obtained by thoses scans. The range was restricted between 45 to 75 A because it provides an appropriate setting region for a high proton beam transmission and a current density operation lower than 3.2 A/mm^2, which is well below the current limit for water-cooled coils of 10 A/mm^2.

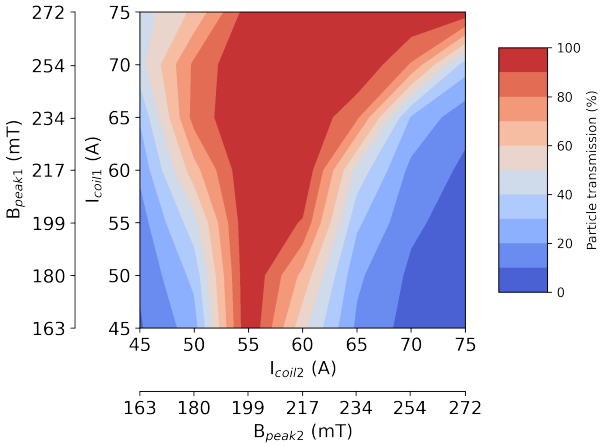

Figure 5: Proton transmission from the solenoid scans. The equivalents B_{peak} fields are also given.

Configurations with high solenoid currents result in higher proton transmission due to a larger magnetic field, resulting in a more compact beam. For settings with I_{coil1} higher than 60 A and I_{coil2} values larger than 55 A, larger transmission is registered. Notably, for configurations with I_{coil2} around 55 A, high transmission is obtained for almost any value of I_{coil1}, which pointing out the importance of the proper focusing of the last solenoid.

Table 4: Cases with more than 90% of Proton Transmission

Case	**I_{coil1} (A)**	**I_{coil2} (A)**
1	45	55
2	50	55
3	55	55
4	60	55
5	60	60
6	65	55
7	65	60
8	70	55
9	70	60
10	70	65
11	75	55
12	75	60
13	75	65
14	75	70
15	75	75

Table 4 shows cases with transmission over 90%. The beam performance of these cases was analyzed and com-

pared to identify suitable candidates for RFQ models (yellow areas), as shown in Fig. 6. Proton transmission is increased by increasing solenoid current but causes high-charge ions transmission too. We are interested in the region with high proton transmission but low high-charge ions transmission. In addition, high-current solenoids will keep the beam small, thus reducing the emittance growth by no-linear fields. The requirements more restricted were a convergence beam (positive α) and a small beam size (small β), see Table 1.

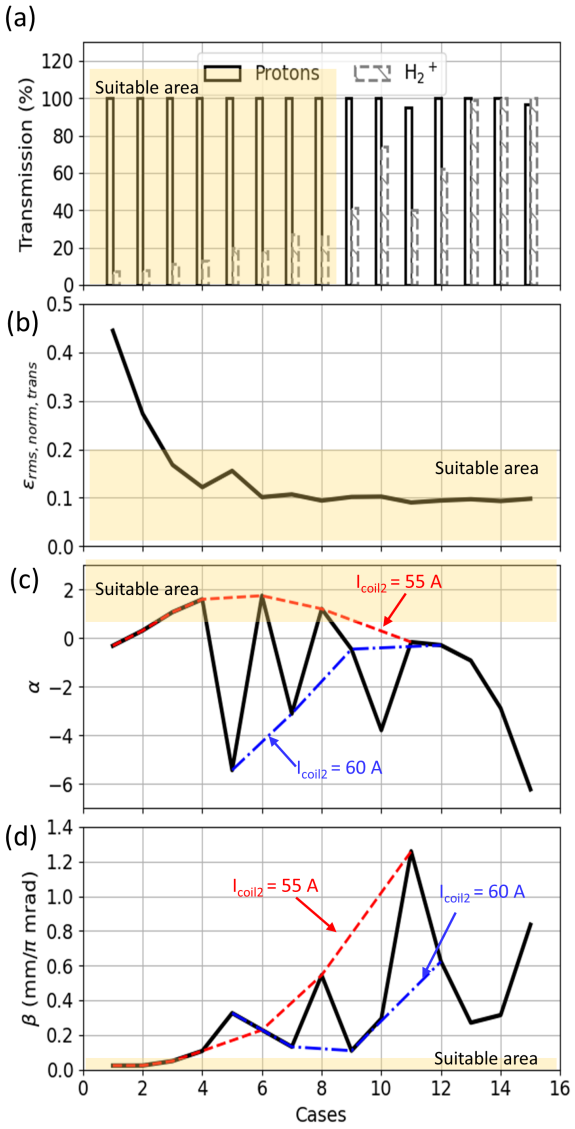

Figure 6: Beam performance for the interested cases: (a) Proton and H_2^+ transmission, (b) Twiss β, (c) $\epsilon_{rms,norm,trans}$, and (d) Twiss α. The yellow areas indicate the suitable performance required for the RFQ models. In addition, the trending for models with second coil current of 55 A (red-dashed line) and 60 A (blue-dashed-dot line) are plotting on the subplots (b) and (c).

Based on the analysis, cases 3 and 4 were chosen as inputs for the RFQ models since they had the most suitable performance. Table 5 displays the beam performance for the accepted cases. For the Reference RFQ, only a performance comparison with Case 3 is presented in Fig. 7 since the results indicate that Case 3 is acceptable. In the case of EP RFQ, the two cases resulted in an RFQ transmission of over 93%, but there was a considerable increase in longitudinal emittance, as shown in Fig. 8 (b).

Table 5: Beam Parameters for the Cases 3 and 4

Parameter	**Case 3**	**Case 4**
Particle	Proton	
Beam current (mA)	20	
Beam energy (keV)	35	
$\varepsilon_{rms,norm,trans,final}$ (π mm mrad)	0.17	0.12
α	1.1	1.6
β (mm/πmrad)	0.05	0.11

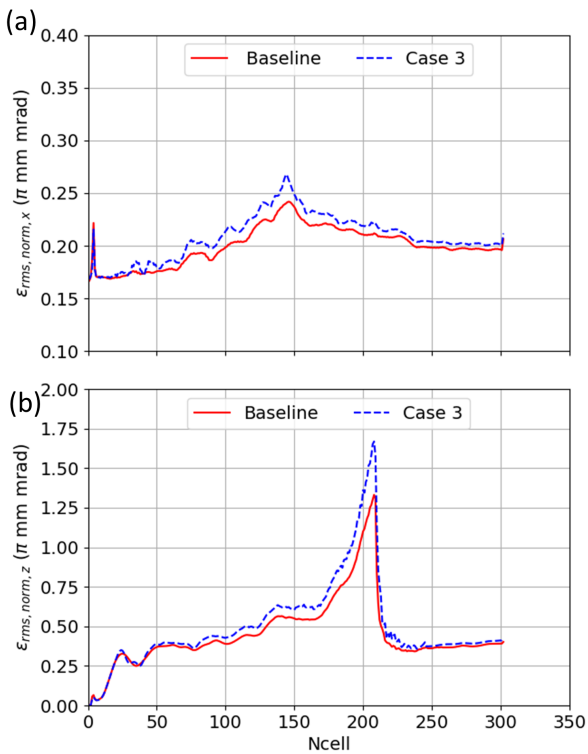

Figure 7: Emittance comparisons for the Reference RFQ model using the baseline (ideal) input parameters and the obtained for the Case 3.

CONCLUSIONS

This work reports the first studies for the LEBT design for the JAEA-ADS linac. The JAEA-ADS LEBT adopted a magnetostatic model using two solenoids to transport the beam

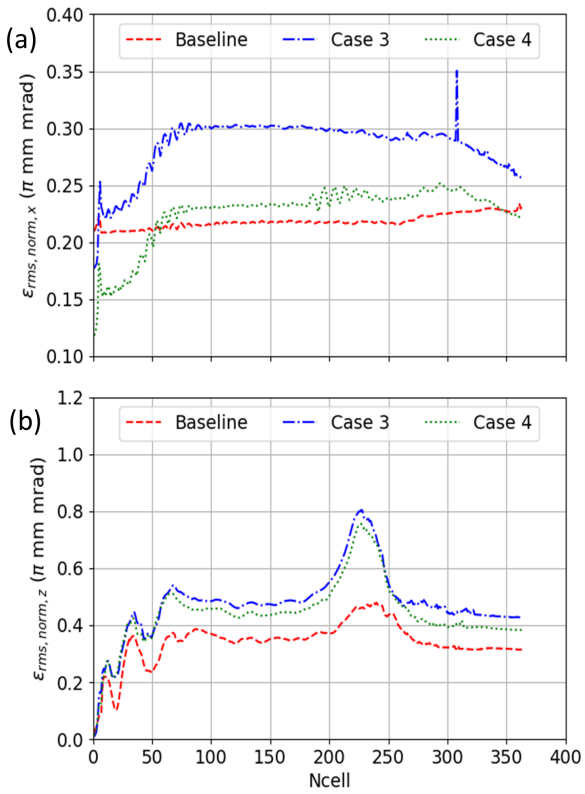

Figure 8: Emittance comparisons for the EP RFQ model using the baseline (ideal) input parameters and the obtained for the cases 3 and 4.

from the ion source to the RFQ. First, a systematic procedure integrating analytical calculations and 3D-EM simulations was developed to design and optimize the JAEA-ADS LEBT solenoid to reduce emittance growth produced by the aberrations. Then, the LEBT design was optimized for the steady state case, i.e., without chopper operation. The simulation studies considered different values of space-charge compensation along the LEBT length. Solenoid current scans were applied to determine optimum values. The analysis found several configurations that provide high proton transmission. Among those cases, Case 3 (I_{coil1} = 55 A and I_{coil2} = 55 A) and Case 4 (I_{coil1} = 60 A and I_{coil2} = 55 A) were used as input for the two RFQ designs for JAEA-ADS: the Reference and EP. The results showed that Case 3 is suitable for the Reference RFQ model. High beam transmission was achieved in cases 3 and 4 for EP RFQ, but further optimizations are needed due to extra emittance growth.

Our next step is to develop a better LEBT design using the WARP code [14], which will help us accurately estimate space-charge compensation and study beam transients.

ACKNOWLEDGMENTS

The authors would like to thank to Nicolas Chauvin, Lorenzo Neri, Cristhian Valerio, Kai Masuda, Takanori Shibata, Hidetomo 0guri, and the members of the JAEA-ADS group for their comments and suggestions.

REFERENCES

[1] T. Sugawara *et al.*, "Research and Development Activities for Accelerator-Driven System in Jaea", *Prog. Nucl. Energy*, vol. 106, p. 27, Feb. 2018. doi:10.1016/j.pnucene.2018.02.007

[2] B. Yee-Rendon *et al.*, "Design and beam dynamic studies of a 30-MW superconducting linac for an accelerator-driven subcritical system", *Phys. Rev. Accel. Beams.*, vol. 24, p. 120101, Dec. 2021. doi:10.1103/PhysRevAccelBeams.24.120101

[3] Y. Kondo *et al.*, "Reference design of the RFQ for JAEA-ADS linac", *JPS. Conf. Proc.*, vol. 33, p. 011015, March 2021. doi:10.7566/JPSCP.33.011015

[4] B. Yee-Rendon *et al.*, "Design and Beam Dynamics Studies of an ADS RFQ Based on an Equipartitioned Beam Scheme", in *Proc. of the PASJ2022*, Online, Japan, Oct. 2022, WEP001, pp. 499-502.

[5] B. Yee-Rendon *et al.*, "Design and Optimization of a Proton Source Extraction System for the JAEA-ADS Linac", in *Proc. of the IPAC2023*, Venezia, Italy, May. 2023, TUPA121, pp. 1573-1575.

[6] N. Chauvin *et al.*, "Source and Injector Design for Intense Light Ion Beams Including Space Charge Neutralisation", in *Proc. of the LINAC2010*, Tsukuba, Japan, Sept. 2010, TH302, pp. 740-744.

[7] L. Bella, "Beam Dynamics Characterization of the IFMIF/EVEDA RFQ Input Beam", Ph.D. thesis, Physics and Astronomy Dept. Univesita degli Studi di Padova, Padova, Italy, 2017.

[8] L. Neri *et al.*, "The ESS Low Energy Beam Trasnport Line Design", in *Proc. of the LINAC2012*, Tel-Aviv, Israel, Sept. 2012, THPB028, pp. 912-914.

[9] N. Chauvin and C. Valerio, private communication, May to Jun. 2023.

[10] Y. K. Batygin *et al.*, "Design of low energy beam transport for new LANSCE H^+ injector", *NIM-A*, vol. 753, p. 1, March 2014. doi:10.1016/J.NIMA.2014.03.041

[11] P. Durandeau and C. Fert, "Étude sur les lentilles électroniques magnétiques", *Rev. Opy*, vol. 36, p. 205, 1957.

[12] CST Studio Suite, "CST Microwave Studio," 2020. http://www.cst.com

[13] TraceWin Manual, http://irfu.cea.fr/dacm/logiciels

[14] A. Friedman *et al.*, "Computational methods in the WARP code framework for kinetic simulations of particle beams and plasmas", *IEEE Trans. Plasma Sci.*, vol. 42, p. 1321, June 2013. doi:10.1109/PLASMA.2013.6633427